JOURNAL OF THERMOPHYSICS AND HEAT TRANSFER
Vol. 23, No. 1, January–March 2009

Numerical Study of Film-Cooling Performance on a Rotating Model

G. Q. Xu, B. Yang,* Z. Tao, S. T. Ding, and H. W. Wu
Beihang University, 100083 Beijing, People's Republic of China

DOI: 10.2514/1.36982

Flow characteristics, adiabatic effectiveness, and discharge-coefficient distributions are numerically investigated on a rotating film-cooling model under different operating conditions. The computational model originates from the midspan section of a typical turbine rotor with two rows of 14 staggered injection holes angled at 30, 60, and 90 deg, on both the suction surface and pressure surface, and the flow through the coolant plenum and all of the hole pipes are resolved as a part of the computational domain by specifying the coolant mass flux in the plenum. The commercial computational fluid dynamics code Star-CD with structured body-fitted grids is employed for the computations, and the Wilcox κ-ω model is chosen for turbulence closure. In the present study, the Reynolds number *Re* based on mainstream velocity and injection-hole diameter varies from 1835 to 5507, and the averaged blowing ratio *M* ranges from 0.5 to 1.5. Results show that the coolant will move to the high-radius locations near the suction and pressure surfaces due to the strong centrifugal effect, which leads to the decrease in adiabatic effectiveness accordingly. The discharge coefficients C_d on the pressure surface are much higher than those on the suction surface under a given operating condition. In addition, the critical values of angular speed that represent the equilibrium of centrifugal force and Coriolis force near the pressure surface are also presented in this paper.

Nomenclature

B	=	space between two rows
C_d	=	discharge coefficient
D	=	film-cooling-hole diameter
Ec	=	Eckert number
L	=	length of the hole pipe
M	=	averaged blowing ratio $[(\rho_c u_c)/(\rho_g u_g)]$
m	=	mass flow rate
P	=	Pressure
Pr	=	Prandtl number (v/a)
R	=	gas constant
Re	=	Reynolds number $(u_g D/v)$
Rt	=	rotation number $(\Omega D/u_g)$
S	=	distance between holes in a row
T	=	temperature
Tu	=	turbulence intensity
u	=	velocity
u^*	=	shear velocity
X^*	=	dimensionless coordinates
x, y, z	=	Cartesian coordinate system with z coordinate along the span
y^+	=	distance in wall coordinates (yu^*/v)
a	=	thermal diffusivity
η	=	film-cooling effectiveness $[(T_g - T_{aw})/(T_g - T_c)]$
v	=	kinematic viscosity
ρ	=	density
φ	=	inclination angle to wall surface
Ω	=	angular speed

Subscripts

aw	=	adiabatic wall
c	=	coolant
g	=	mainstream
w	=	wall

Received 3 February 2008; revision received 7 August 2008; accepted for publication 22 October 2008.

*National Key Laboratory on Aero-Engines, School of Jet Propulsion; yb1982@sjp.buaa.edu.cn.

I. Introduction

FILM cooling is commonly used as an effective cooling technique to prevent turbine blades from thermal failure caused by operation in a high-temperature environment. In the case of film cooling, the cooler air is injected into the high-temperature mainstream boundary layer on the blade surface and generates a thin coolant film acting as a buffer to isolate the thermal loads. With the aid of film cooling, a higher gas temperature at the turbine inlet is permitted, which in turn greatly improves the thermal efficiency of the turbine engines.

Various fluid dynamics and geometric parameters can affect the performance of film cooling, such as the mainstream Reynolds number; blowing ratio; coolant-to-mainstream density ratio; turbulence intensity; film-hole shape, size, and location, etc. Therefore, achieving a comprehensive understanding of the film-cooling technique as well as efficient design of the film-cooling modes has become a very important issue. The present work is conceived as a contribution to study the film-cooling mechanism and to develop the predictive capability to be used in the design process.

Many studies have been conducted on the performance of film cooling over the past four decades, and a large amount of the valuable results is available in the open literature. An excellent review of the film-cooling work up to 1971 was provided by Goldstein [1]. Many efforts have been devoted afterward to this research area, and a comprehensive compilation of the achievements has been summarized by Han et al. [2]. Some of the relevant experimental and computational work found in the open literature is summarized subsequently.

Sinha et al. [3] investigated two rows of 35 deg holes with a pitch-to-diameter ratio of 3 and a row spacing-to-diameter ratio of 40 film-cooling performances. They found that the upstream row thickened the boundary layer between the two rows, reduced the momentum of the crossflow and the velocity gradients in the shear layers, and lowered the turbulence level for the second row. Baldauf et al. [4] employed a high-resolution thermography system to study the local adiabatic film-cooling effectiveness on a flat-plate surface downstream of a row of cylindrical injection holes. In their experiment, the streamwise inclination angle varied from 30 to 90 deg, and the blowing ratio ranged from 0.2 to 2.5. It was found that

the optimum conditions were confined to a small band of blowing ratios around $M = 0.85$ to 1.0 and momentum ratios of $I = 0.4$ to 0.5. Harrington et al. [5] conducted an experimental investigation on the film-cooling adiabatic effectiveness of a flat plate with full-coverage film cooling. Results showed that the optimum adiabatic effectiveness was found to occur for a blowing ratio of $M = 0.65$. Ahn et al. [6] measured the boundary-layer temperature and adiabatic film-cooling-effectiveness distributions to describe the injectant behaviors from two rows of film-cooling holes with opposite orientation angles. Results showed that the injectant was centered near the film-cooled surface irrespective of hole configurations at the blowing ratio of $M = 0.5$, but the interaction between cooling jets from the upstream and downstream holes became important for film-cooling effectiveness at the higher blowing ratios of $M > 1.0$. Saumweber and Schulz [7] conducted a comprehensive set of generic experiments to investigate the interaction of film-cooling rows. They considered five different film-cooling configurations on a large-scale basis, each consisting of two rows of injection holes in staggered arrangement, and found that the decay of film-cooling effectiveness with streamwise distance was much less pronounced downstream of the second row, primarily due to precooling of the boundary layer by the first row of holes. Kim et al. [8] investigated the detailed local heat transfer and film-cooling-effectiveness distributions from a trailing-edge model of a gas turbine airfoil in a low-speed wind tunnel. They found that both local heat transfer coefficients and film-cooling effectiveness displayed a strong dependency on the blowing ratio and mainstream acceleration. However, the discharge coefficients showed little dependency on the mainstream acceleration. Yuen and Martinez-Botas [9,10] studied the film-cooling effectiveness and heat-transfer-coefficient distributions on rows of cylindrical holes with streamwise angles of 30, 60, and 90 deg in a flat-plate test facility with zero pressure gradient. They concluded that the optimum value of blowing ratio was about 0.5 for most configurations, and the small pitch-to-diameter ratios and inclination angles were prone to offer better protection over the wall surface.

In addition to the experimental film-cooling studies outlined earlier, many efforts in computational approaches have also been devoted to the film-cooling characteristics. A number of parametric studies were provided by Garg and Gaugler [11] Garg [12], Garg and Gaugler [13,14] ; to investigate the effects of several parameters, such as the effect of coolant velocity and temperature distributions at the hole exit, the effect of blade rotation and the direction of coolant ejection from the showerhead holes, the effect of spanwise pitch of the showerhead holes, and the effect of coolant-to-mainstream mass flow and temperature ratio.

Leylek and Zerkle [15] studied the discrete hole film-cooling on a flat plate using the standard κ-ε turbulence model with wall functions for $DR = 2$ and L/d of 1.75 and 3.5. Following the coolant from the plenum into the hole pipe, they presented the coolant velocity and temperature profiles at the hole exit. By using the same turbulence model, Giebert et al. [16] analyzed the flowfield at the exit of cylindrical and shaped injection holes on a flat plate. Compared with the measured mean velocity and turbulence quantities, they found a decided difference inside the hole and at the hole exit. Lakehal et al. [17] investigated the film-cooling effectiveness of a flat plate by a row of laterally injected jets using a Navier–Stokes equation solver that employed a finite volume method with a multiblock technique. Their work compared the measured and calculated temperatures and velocity fields obtained with the standard κ-ε and the κ-ε based on the two-layer turbulence model for various blowing ratios. Compared with the results obtained with wall functions, they found that the resolution of the viscosity-affected near-wall region with a one-equation turbulence model yielded a noticeable improvement in the prediction of film-cooling effectiveness. Azzi and Lakehal [18] simulated the streamwise injection of film coolant over a flat plate for a density ratio of 2 and mass flux ratios of 0.5 and 1.0. They employed various turbulence models to simulate the turbulent exchange processes. Results showed that the isotropic two-layer κ-ε model was found to underpredict the lateral spreading of the temperature field, together with an exaggerated size of the kidney vortices. Garg and Rigby [19] used a multiblock three-dimensional Navier–Stokes code with a κ-ω turbulence model to study the within-hole and near-hole behaviors in relation to heat transfer on a film-cooled blade. It was found that the coolant velocity and temperature distributions at the hole exit on the blade side did not follow the one-seventh power-law profile and were highly skewed by the mainstream for the holes close to the leading edge of VKI rotor. Tyagi and Acharya [20] performed an accurate prediction of the flowfield by large eddy simulations for a row of inclined cylindrical holes at blowing ratios of 0.5 and 1.0 and Reynolds numbers of 11,100 and 22,200, respectively, based on the jet velocity and hole diameter. The calculated results showed that the unsteady three-dimensional flowfield was significantly dominated by the packets of hairpin-shaped vortices. To obtain more accurate results, Muldoon and Acharya [21] computed the film-cooling performance of an inclined injection hole by using the direct numerical simulation approach. Finally, they concluded that the great weakness in the standard κ-ε model was the choice of eddy viscosity.

All studies described so far have already shown many significant results in static film cooling. In the open literature, however, little academic research has been reported to investigate the film-cooling performance under rotating engine conditions. In gas turbine engines, the flow patterns induced by the intense turbulent mixing process of the cooling jets in the mainstream are strongly influenced by the rotational effect, which directly results in the distinct features of film cooling.

Dring et al. [22] studied the adiabatic film-cooling effectiveness on the rotor blade of a large-scale (low-speed) model for a high-pressure turbine's first stage. The coolant was discharged from single holes on the pressure and suction surfaces of the airfoil. Their results showed that the film coolant had only a small radial displacement, similar to flat-plate results, on the suction surface. But on the pressure surface, the coolant trace had a large radial displacement toward the blade tip due to rotation, and a much faster decay of the effectiveness was observed. Takeishi et al. [23] measured the adiabatic effectiveness on a low-speed stationary cascade and a rotating blade by using the heat-mass transfer analogy. They reported that the adiabatic effectiveness on the suction surface of the rotating blade agreed well with that on the stationary blade, but a low level of effectiveness appeared on the pressure surface of the rotating blade. Abhari and Epstein [24] studied the time-resolved heat transfer characteristics for cooled and uncooled rotors by thin heat flux gages, and Ahn et al. [25] measured the film-cooling-effectiveness distributions on the leading-edge region of a rotating blade using a pressure-sensitive-paint technique. As a further study, Ahn et al. [26] reported that different rotating speeds can change the film-cooling traces distinctly, with the averaged film-cooling effectiveness on the leading-edge region increasing with blowing ratio. Yang et al. [27] employed a Reynolds stress turbulence model together with a nonequilibrium wall function to calculate the film-cooling effectiveness and the associated heat transfer coefficients on the leading edge of a rotating blade in a particular turbine stage. Results showed that the heat transfer coefficients increased, but film-cooling effectiveness decreased with increasing rotating speed. Furthermore, a series of computational studies on the heat transfer characteristics for a film-cooled rotating blade by using different turbulence models were also conducted by Garg and Abhari [28] and Garg [29,30].

To better understand the mechanism of film-cooling phenomenon under rotating operating conditions, both studies concerning the performance on the entire turbine blade and features on physical model are extremely important. So far, some studies have contributed to comprehend the cooling performance on the entire turbine blades, but not much information is reported in the published literature on the contribution of understanding the coolant mechanism on physical models. Therefore, from the mechanism research point of view, the general purpose of the present work aims to investigate the rotational effect on the film-cooling performance. To facilitate the analysis of focal points, some other parameters (such as the pressure gradient, surface curvature, and compound angle) are not taken into account, and the influences of several leading parameters (i.e., mainstream Reynolds number, blowing ratio, and

rotation number) on the film-cooling performance are emphasized. By means of the computational fluid dynamics (CFD) approach, the flow characteristics and cooling effectiveness on a simplified rotating film-cooling model with two rows of 14 staggered injection holes are investigated, and the discharge-coefficient distributions for all of the hole pipes are also obtained. The computed results will be greatly helpful to explore the film-cooling phenomenon in gas turbine engines.

II. Methodology

A. Theoretical Analysis

The cooling performance of a film-cooled surface is most commonly described by the adiabatic film-cooling effectiveness η, which is defined as a nondimensional temperature:

$$\eta = (T_g - T_{\text{aw}})/(T_g - T_c) \tag{1}$$

where T_g is the mainstream temperature, T_c is the coolant temperature, and T_{aw} is the adiabatic wall temperature.

After processing the flow and heat transfer governing equations and boundary conditions in the rotating reference frame on a film-cooled blade model, the dimensionless group to the adiabatic effectiveness η can be summarized as follows:

$$\eta = f(Re, Rt, Ec, Pr, M, P_c/P_g, \rho_c/\rho_g, \varphi, X^*) \tag{2}$$

where Re is the Reynolds number based on mainstream velocity and injection-hole diameter, Rt is the rotation number, Ec is the Eckert number, Pr is the Prandtl number, M is the blowing ratio, P_c and P_g are the coolant pressure and mainstream pressure, ρ_c and ρ_g are the coolant density and mainstream density, φ is the inclination angle, and X^* is the dimensionless coordinates. The present work aims to concentrate on the influence of leading parameters Re, M, and φ on the performance of film-cooling under rotating operating conditions.

B. Rotating Film-Cooling Model

A schematic illustration of the rotating film-cooling model, which originates from the midspan section of a typical turbine rotor and simplified properly, with two rows of staggered injection holes located on both the pressure and suction surfaces for the case of $\varphi = 90$ deg is shown in Fig. 1. The coordinate system used is such that the x axis is along the streamwise direction of the mainstream, the y axis is along the direction of injection holes, and the z axis conforms with the right-hand law. The entire model occupies a space of $0.12 \times 0.082 \times 0.05$ m, and the cutting plane normal to the x axis is a trapezoid with a top angle of 74.6 deg. As can be seen in Fig. 1, the air domain consists of the mainstream and coolant, which are mixed at the exit of injection holes, and the interior part forms the solid domain. The whole model is symmetric to the rotating axis that is parallel, but at a distance of 0.5 m under the x axis. The mainstream has a high temperature and velocity when the hot air reaches the two main inlets with a cross section of 0.028×0.05 m, and the coolant has a low temperature and constant mass flux when the cooling air enters the coolant inlet with a cross section of 0.02×0.01 m, which is at the bottom of the inner plenum. All of the air flows out from the two main outlets. A total of 14 discrete cylindrical holes are designed on the pressure and suction surfaces for film cooling. To investigate the coolant interaction and discharge-coefficient distributions, the injection holes are arranged in two staggered rows. The first row of 4 holes and the second row of 3 holes have a diameter D of 2 mm, and the holes in each row are spaced three hole diameters apart ($S/D = 3$). The space between two rows is $B/D = 4$, and the staggered distance is $1.5D$. Three inclination angles to the pressure and suction surfaces are arranged at $\varphi = 30$, 60, and 90 deg, giving the length-to-diameter ratio $L/D = 6$, 3.46, and 3, respectively. For the present model, the air domain extends from $13D$ upstream of the first row of holes and $43D$ downstream of the second row of holes, and this length scale is sufficient to simulate the flow behaviors of cooling jets in the near-field region of the film hole. The maximum turbulent boundary-layer thickness on the pressure surface is taken to be about 5% of the surface length and $0.7D$ at the injection-hole locations. This model rotates at constant angular speeds of 1000, 2000, and 3000 rpm, respectively. Within this range of rotating speed, the development of the coolant-deflection phenomenon can be distinctly investigated.

C. Grid Generation and Boundary Conditions

The locally structured and body-fitted grid with hexahedral cells was employed and is shown in Fig. 2. Before starting the computation, the grid was tested repeatedly through altering the computational parameters and it can always lead to a converged solution. The grid consisted of $122 \times 130 \times 126$ nodes in the x, y, and z directions and maintained high-quality, smoothness, and near-orthogonality. By using the hexahedral meshing, the grid conveniently ensured accuracy and clusters toward the boundary layers. Normal to the wall surface was the densely viscous grid with $y^+ < 1.2$ for the first grid point, which was strictly kept within the laminar sublayer to satisfy the requirement of a low-Reynolds-number turbulence model. The number of grid points along the pressure and suction surfaces was typically 15 to 20, but less within the hole pipes. To obtain a high-precision-grid solution, the O-grid technique was applied in all of the injection holes and much attention was paid to keep the grid aspect ratios smaller than 1.3 in any direction. Many tests were carried out to obtain an independent solution during the process of grid refining, including a grid that had 1.5 times as many cells as this one in the streamwise direction. The two grids yielded nearly identical adiabatic effectiveness and pressure distributions on the pressure and suction surfaces, and the maximum discrepancy in wall-temperature prediction was within $\pm 1\%$ for all of the tested grids and $\pm 0.6\%$ for almost all of the cases.

The velocity boundary conditions to the mainstream and coolant inlet planes are summarized in Table 1. Here, we should point out that the mass fluxes streaming out from all of the injection holes are assumed to be equal when the velocity at coolant inlet is specified at a fixed value of M. As a consequence, the averaged blowing ratio M could be an ideal flux distribution for coolant. The mainstream had a temperature of 363 K with turbulence intensity of $Tu = 5\%$ after it reached the two main inlet planes, and the coolant had a temperature of 333 K with turbulence intensity of $Tu = 1\%$ in the plenum. When the mixed air streamed out from the two outlet planes, the back pressure was fixed to 101,325 Pa accordingly. Because the mainstream is designed to simulate the flow between neighboring turbine blades, the top and bottom surfaces of the mainstream were set to free-slip walls, and two planes in the exterior of this part were considered as periodic interfaces. In addition, the adiabatic no-slip condition was enforced at all of the solid walls, including the inner surface of the film hole and the inner plenum.

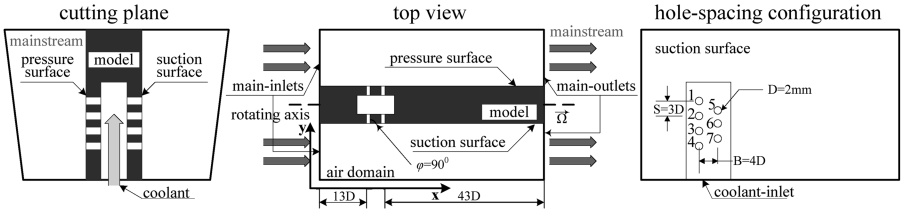

Fig. 1 Schematic of the rotating model and film-hole configuration ($\varphi = 90$ deg).

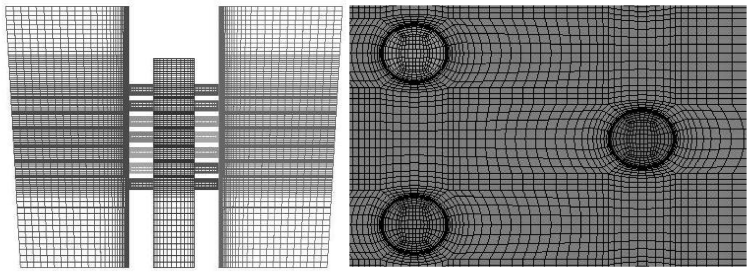

a) Lateral view b) O-grid in hole

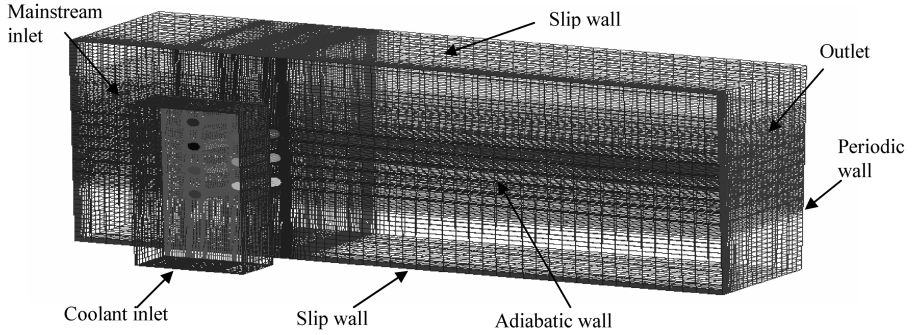

c) Half of computational grid

Fig. 2 Grid used for the computation ($\varphi = 60$ deg).

D. Turbulence Model and Computational Details

In the previous studies, many investigations have been conducted to inspect the actual effect of turbulence models (Azzi and Lakehal [18], Garg and Rigby [19], Garg and Abhari [28], Garg [29,31], Garg and Ameri [32], Hoda and Acharya [33]). Generally, neither the traditional eddy-viscosity models nor Reynolds stress models could provide a systematic closure approach with approving accuracy. Note that the main difficulty in film-cooling simulations is that the flow is considerably anisotropic, particularly in the region surrounding the jet exit and very close to the wall, underneath the secondary vortices. Eddy-viscosity models with wall functions are apt to produce underpredicted results when calculating the lateral spreading of the temperature field and near-wall heat transfer. Following the advice of Garg [29], the κ-ω turbulence model of Wilcox [34] was still chosen because it satisfies many constraints such as asymptotic consistency near walls without the need for additional corrections, and it can also give reasonable results for subsonic flows with adverse pressure gradients, separation, and streamline curvature.

In the present study, the numerical simulations were performed using the commercial CFD code Star-CD, a finite-control-volume-based multiblock and multigrid solver. The flow is assumed to be compressible, and the pressure, density, and temperature are related by using the ideal-gas law. The solutions were obtained by solving the three-dimensional Navier–Stokes equations under the rotating-coordinate system, and the pressure-velocity coupling is achieved by using the well-known SIMPLE (semi-implicit method for pressure-linked equations) algorithm. The standard κ-ω model in conjunction with the scalable wall function was used for turbulence closure, and a high-resolution scheme was employed for discretization of the advection term. Convergence in all cases was declared only when both strict criteria were satisfied:

1) There was a reduction in all residuals of at least 4 orders of magnitude.

2) There was no observable change in the monitored parameters of temperature, velocity, and pressure in the flowfield for an additional 40 iterations.

Further study with enhanced convergence criteria was also performed, and results showed that hardly any variation on adiabatic effectiveness was found. To improve the computational efficiency, the calculations were run on the cluster of 16 parallel processors on PC Pentium 4, 2.4 GHz machines with 16,384 MB memory at Beihang University, Aero-Engines National Key Laboratory, China. A single iteration took approximately 35 s, and about 1100 iterations were required for convergence at each simulated case.

Table 1 Velocity at inlet planes in computation

u	$M = 0.5$	$M = 1.0$	$M = 1.5$
$u_g = 20.3$, m/s	$u_c = 20.6$, m/s	$u_c = 4.13$, m/s	$u_c = 6.19$, m/s
$u_g = 40.6$, m/s	$u_c = 4.13$, m/s	$u_c = 8.25$, m/s	$u_c = 12.38$, m/s
$u_g = 60.9$, m/s	$u_c = 6.12$, m/s	$u_c = 12.23$, m/s	$u_c = 18.34$, m/s

III. Results and Discussion

A summary of the leading fluid dynamics and geometrical parameters in the present study is shown in Table 2.

A. Flow and Temperature Fields

Figure 3 presents the adiabatic film-cooling-effectiveness distributions on the suction surface for various Rt and φ. The particular cases shown here are $M = 0.5$ and $Re = 1835$. To deliver a better understanding of the flowfield, a horizontal line is marked through the center of hole 6 as a reference, and the downstream exit of this hole is located at $x = 0$. A particular phenomenon in rotating film-cooling performance is that the coolant will move to the high-radius locations after it streams out from the cooling holes, especially at high angular speeds. It is well known that there are three governing forces in the rotating system: that is, the centrifugal force, the Coriolis

Table 2 Leading parameters in computation

Parameters	Values
Re	1835, 3671, 5507
Rt	0.0034–0.0309
M	0.5, 1.0, 1.5
φ	30, 60, 90 deg

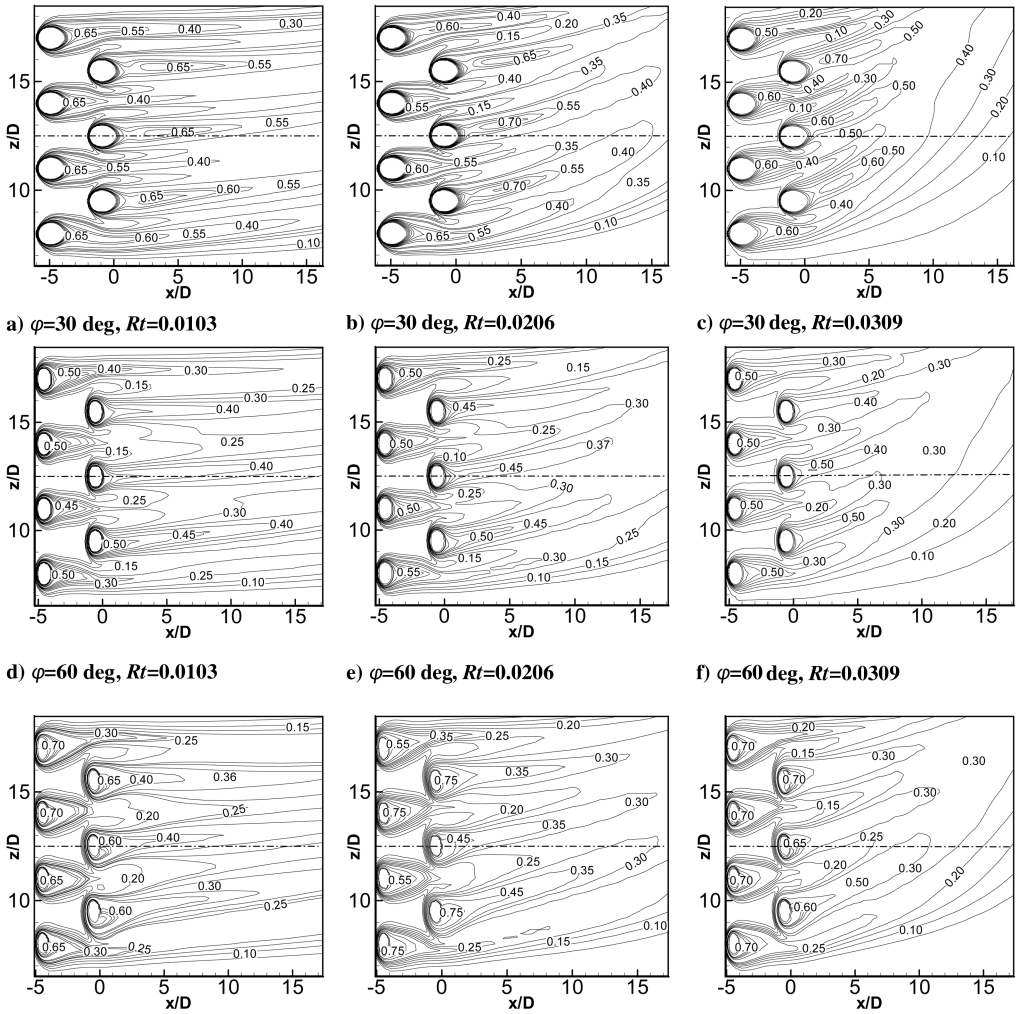

a) φ=30 deg, Rt=0.0103 b) φ=30 deg, Rt=0.0206 c) φ=30 deg, Rt=0.0309

d) φ=60 deg, Rt=0.0103 e) φ=60 deg, Rt=0.0206 f) φ=60 deg, Rt=0.0309

g) φ=90 deg, Rt=0.0103 h) φ=90 deg, Rt=0.0206 i) φ=90 deg, Rt=0.0309

Fig. 3 Contours of film-cooling effectiveness on the suction surface at $Re = 1835$ and $M = 0.5$.

force, and the buoyancy force. The buoyancy force is induced through the former two forces and temperature field, and in the current study, it can be negligible for the small differential of temperature between the mainstream and coolant. The centrifugal force is prone to drive the air to deflect toward the high-radius locations, especially for the high-density coolant, whereas the Coriolis force pushes the cooling jets upward and downward along the z-axis direction near the suction and the pressure surfaces, respectively. As a result, the coolant deflection near the suction surface is more evident. The adiabatic effectiveness distributions in Fig. 3 can be very helpful to analyze the coolant-deflection phenomenon. It can be clearly seen that as Rt increases from 0.0103 to 0.0309, the contour at $\eta = 0.5$ downstream of the second row of holes is deflected about $3.5D$ upward at $x/D = 8$ ($\varphi = 30$ deg), and the effective region covered by cooling film tends to decrease in both the x and z directions (see Figs. 3a–3c). In addition, the decreasing tendency becomes more evident with the increase of the inclination angle φ. Through comparisons for the different φ, the $\varphi = 30$ deg cases present the best protection to the wall surfaces at $M = 0.5$, and the regions of high η values ($\eta \geq 0.5$) extend to $15D$ locations along the x-axis direction, whereas the same regions end within the farthest distances of $x = 4D$ at $\varphi = 60$ deg and even $2D$ at $\varphi = 90$ deg. Because of the interaction of cooling jets from two rows of injection holes, the thermal protection between two neighboring holes of the second row along the z-axis direction is the best at $\varphi = 30$ deg, followed by a subsequent decrease at $\varphi = 60$ and 90 deg. This result also agrees with the study conducted by Yuen and Martinez-Botas [9].

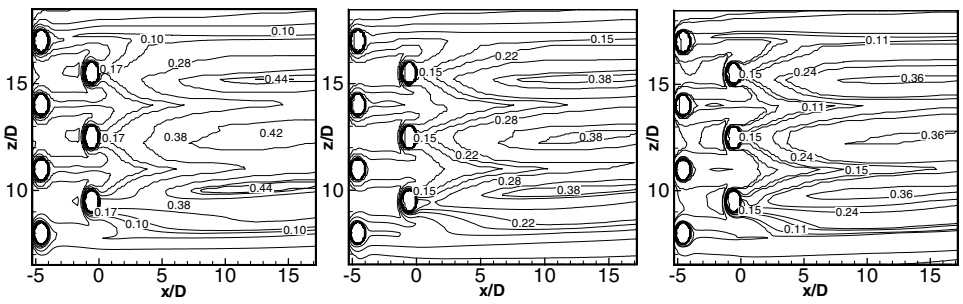

a) Re = 1835 b) Re = 3671 c) Re = 5507

Fig. 4 Adiabatic film-cooling-effectiveness distributions on the pressure surface at $M = 1.0$ and $Rt = 0.0103$ ($\varphi = 60$ deg).

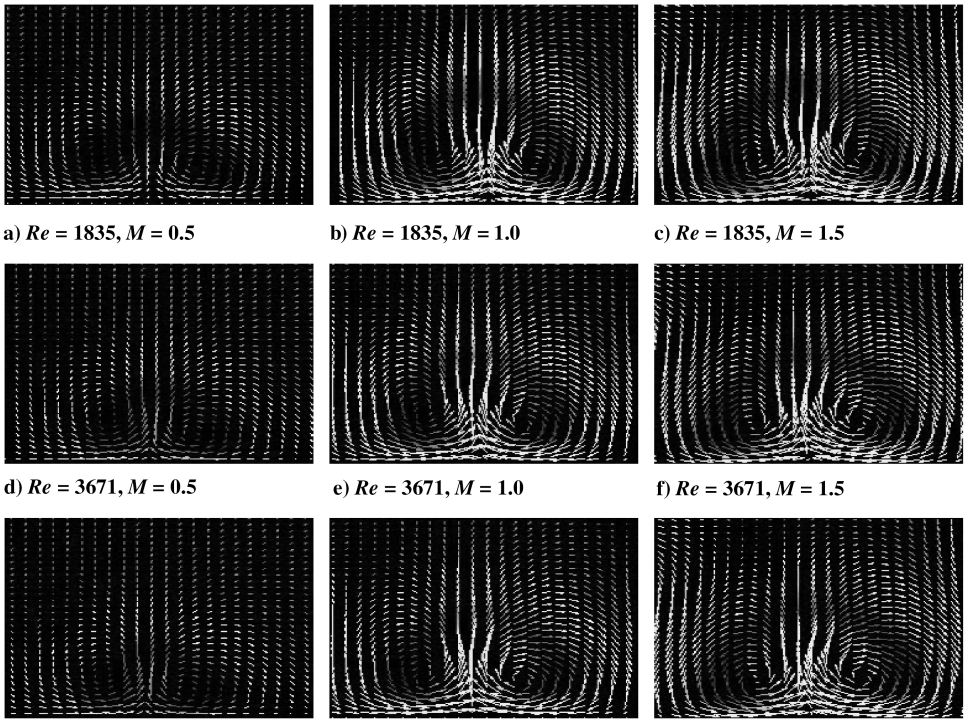

a) $Re = 1835, M = 0.5$ b) $Re = 1835, M = 1.0$ c) $Re = 1835, M = 1.5$

d) $Re = 3671, M = 0.5$ e) $Re = 3671, M = 1.0$ f) $Re = 3671, M = 1.5$

g) $Re = 5507, M = 0.5$ h) $Re = 5507, M = 1.0$ i) $Re = 5507, M = 1.5$

Fig. 5 Vector illustration for counter-rotating vortices normal to the suction surface at $Rt = 0.0103$.

Figure 4 presents the contours of adiabatic effectiveness on the pressure surface with the variation of the Reynolds number at $Rt = 0.0103$ and $M = 1.0$. The values of η downstream of the second row holes seem to vary slightly when the Reynolds number increases from 1835 to 5507, which implies that the adiabatic effectiveness appears to be insensitive to the variation of Reynolds numbers under a given operating condition.

Figure 5 is a vector illustration for the cooling jets along a cross section normal to the suction surface at $x = 2D$ location downstream of the injection hole 6. An important feature in the film-cooling flowfield is the formation of highly complex counter-rotating vortices (CRVs) near the wall surface due to the strong lateral component of the mainstream and outward flow of the coolant. As a result of vortex induction, the CRVs cause the jets to lift off from the wall surface and entrain hot gases from the surroundings to the surface, which leads to a hot streak on the wall surface along the centerline. Therefore, the goal in design of film-cooling strategies is to keep the cooling jets attached to the wall surface as far downstream as possible with minimal entrainment of hot gases to avoid the hot streak. From Fig. 5, it can be observed that the vortices are the smallest for $M = 0.5$ and expand with the increase of blowing ratio to a value of $M = 1.5$ under constant-Reynolds-numbers conditions. The interaction of the mainstream and cooling jets is reduced, leading to a weak secondary flow structure due to the decreased momentum of the cooling jets for $M = 0.5$, and the displacement of the cores in the cooling jets is the closest near the surface, which means that more effective protection to the wall surface is achieved. As Rt increases, the CRVs move upward along the z-axis direction, embodying the action of centrifugal force. Differing with the shape under the static condition, the vortex system is not perfectly symmetric, and this is in line with the study of Bohn et al. [35]. After a detailed comparison with all of the cases, little changes are found when Rt alters, but the increase of Reynolds number seems to result in an enlargement of the CRVs.

Figure 6 shows the jet-to-mainstream-penetration vector graphs near the suction surface after injection hole 6. Usually, if the blowing ratio M is less than some critical values depending on geometry and operating conditions, then the cooling jet stays attached to the wall surface when exiting the film-cooling hole. But if M reaches a high value beyond the critical values, the detachment and reattachment phenomena will play an important role in the flowfield. Because the coolant at high values of M has a much greater momentum normal to the mainstream, it penetrates into the mainstream easily at the hole exit and then reattaches to the wall surface after separation and passing an appropriate distance along the streamwise direction. From Fig. 6, it can be observed clearly that a recirculation region exists downstream of the injection hole in the $\varphi = 90$ deg case, a faint one in the $\varphi = 60$ deg case, and hardly any for the $\varphi = 30$ deg case, due to the smallest inclination angle. The pressure within this region is much lower than that in the mainstream region, especially near the

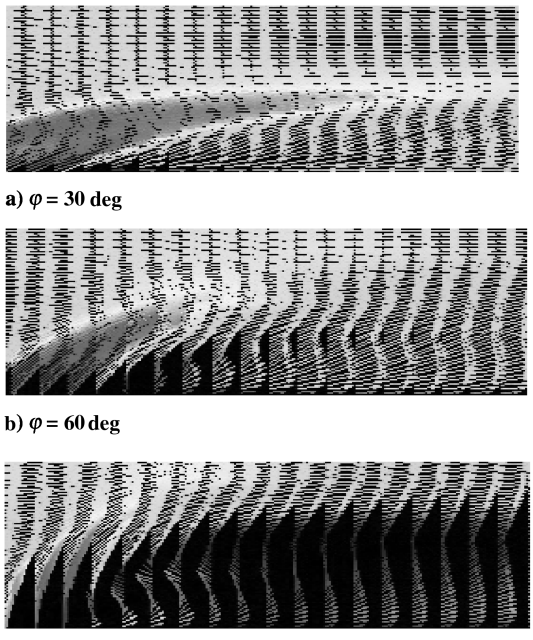

a) $\varphi = 30$ deg

b) $\varphi = 60$ deg

c) $\varphi = 90$ deg

Fig. 6 Illustrations of the jet penetration on the suction surface ($Re = 3671, Rt = 0.0155, M = 1.5$).

Table 3 Theoretical values for CAS ($\varphi = 30$ deg)

Re	$M = 0.5$	$M = 1.0$	$M = 1.5$
$Re = 1835$	168 rpm	335 rpm	502 rpm
$Re = 3671$	335 rpm	670 rpm	1005 rpm
$Re = 5507$	502 rpm	1005 rpm	1507 rpm

hole exit, due to the existence of an adverse pressure gradient, and the temperatures here are higher than in surrounding regions.

As described earlier, the centrifugal force and Coriolis force present opposite effects on coolant movement near the pressure surface. To distinguish the most dominating factors in the coolant-deflection phenomenon in film-cooling, the classical boundary-layer theory is introduced into the momentum equations. It can be derived that the movement of coolant flow is dominated by four primary governing forces: that is, pressure gradient, viscosity force, Coriolis force, and centrifugal force. For the present study, it is assumed that the pressure gradient and viscous stress could be omitted in the z-direction momentum equation for their small quantity when compared with the other two governing forces, and then the coolant can be influenced only by the Coriolis force and centrifugal force to deflect along the radial direction. When the Coriolis force plays a dominant part in the flowfield at low angular speeds, the coolant will move to the low-radius locations near the pressure surface; whereas the centrifugal force is enhanced with the increase of angular speed, the coolant will move back to the upward locations again. Therefore, there should exist a critical value of angular speed (CAS) at which the two governing forces are equivalent and their action to the coolant can be counteracted mutually. Focusing on a random particle of cooling jets at the exit of the injection hole, the equilibrium equation can be established as follows:

$$2\rho\boldsymbol{\Omega}u_c \sin\varphi = \rho\boldsymbol{\Omega}^2 z \tag{3}$$

from Eq. (3), taking $\varphi = 30$ deg as an example, the theoretical solutions of CAS can be obtained for various Reynolds numbers and M, as listed in Table 3. To validate the CAS assumption, the adiabatic effectiveness based on a test point that is located at $x = 6D$ along the centerline of hole 5 was investigated and is shown in Fig. 7. This film hole was chosen because of its high-radius location and less interaction of cooling jets from neighboring holes. As can be seen in Fig. 7, because the Coriolis force plays a leading role on the coolant movement, the values of η decrease continually as the angular speed starts to increase. Although a minimum value of η is reached, the adiabatic effectiveness starts to increase again. At this stage, the Coriolis force is still dominant, although the difference between Coriolis force and centrifugal force is reduced gradually, due to the augmentation of angular speed. When η returns to the initial value under the static state, the CAS can be obtained. The computed results

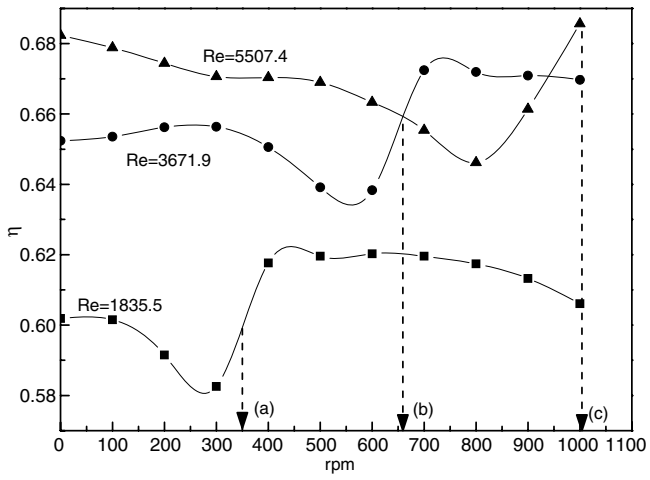

Fig. 7 Computed results for CAS ($M = 1.0$).

of three CAS values for different Reynolds numbers are denoted by points a, b, and c in Fig. 7. Because of the interaction of cooling jets from neighboring injection holes, there is no illustration to show the obvious downward deflection for coolant trajectories through the computation. But we can still take an indirect proof from Fig. 7 to prove the existence of CAS. Considering the different velocity distributions for each cooling-hole exit plane and the omitted terms in the momentum equation, seeking a satisfied theory for CAS is therefore an absolute essential.

B. Film-Cooling Effectiveness

Figure 8 presents the laterally averaged film-cooling-effectiveness results as a function of x/D at the centerline of hole 6 on suction and pressure surfaces under different operating conditions. Through a detailed comparison, the tendencies of η are summarized as follows:

1) The high values of M will weaken the thermal protection to wall surfaces, especially near the exit of cooling holes, but they will increase the adiabatic effectiveness properly at far-downstream locations. The numerical result (Fig. 8a) reveals that an abrupt decrease in the cooling effectiveness η occurs at $x/D < 2$, whereas a further increase in η appears at $x/D = 2$–8. This is due to the fact that the cooling jets detach from the wall surfaces immediately after effusing from the injection holes and then reattach at downstream locations after separation. In this region, the highest η appears at $M = 0.5$. While in the region of $x/D \geq 14$, the η level of $M = 1.0$ and 1.5 is higher than in the $M = 0.5$ case, because the high M values bring an enhanced momentum in coolant, which results in an increase in η at far-downstream locations. In other words, the high values of M lead to a better protection to wall surfaces compared with the case of $M = 0.5$ in this region. The similar tendency of η also appears at $\varphi = 60$ and 90 deg (see Figs. 8d and 8g).

2) Although the values of η next to the downstream locations of injection holes on the suction surface are higher than those on the pressure surface, the adiabatic effectiveness on the pressure surface is much superior to that on the suction surface within most of regions because of the strong deflection of coolant near the suction surface. Both the centrifugal force and Coriolis force point toward the high-radius locations near the suction surface, which allows more coolant to be deflected upward. On the pressure surface, the centrifugal effect will be weakened due to the opposite effect of Coriolis force and it finally leads to the high values of η.

3) As Rt increases, the values of η on both the suction surface and pressure surface decrease simultaneously for the same reason as with coolant deflection (see Figs. 8b, 8e, and 8h). The cooling jets from neighboring injection holes can provide additional compensations for the adiabatic effectiveness because of their intense mixing, which can result in the recovery of η in the far-downstream region of $x/D > 18$.

4) It appears that the augmentation of the Reynolds number can lead to a slight decrease of η at downstream locations (see Figs. 8c, 8f, and 8i). To keep a constant value of Rt, the angular speed should be elevated simultaneously as the Reynolds number increases, which is the exact reason for the reduction of adiabatic effectiveness.

5) After reaching the far-downstream locations, the tendencies of η become more uniform on the suction and pressure surfaces.

Generally, the effect of film cooling at $\varphi = 60$ and 90 deg presents an analogical status, whereas the cooling behavior of $\varphi = 30$ deg shows a distinct representation and a better protection to wall surfaces as a result of the reduced component of the cooling jet's velocity in the y direction.

C. Discharge Coefficient

Knowledge of the discharge coefficient C_d is vital in sizing film-cooling holes at the design stage to determine the requisite amount of coolant flow to produce the desired cooling effectiveness. The discharge coefficient C_d is the ratio of actual mass flow rate and ideal mass flow rate through the film-cooling hole. The ideal mass flow rate is calculated assuming an isentropic one-dimensional expansion from the total pressure in the coolant supply P_{tc} to the static pressure in the mainstream P_g. Therefore, C_d can be expressed as

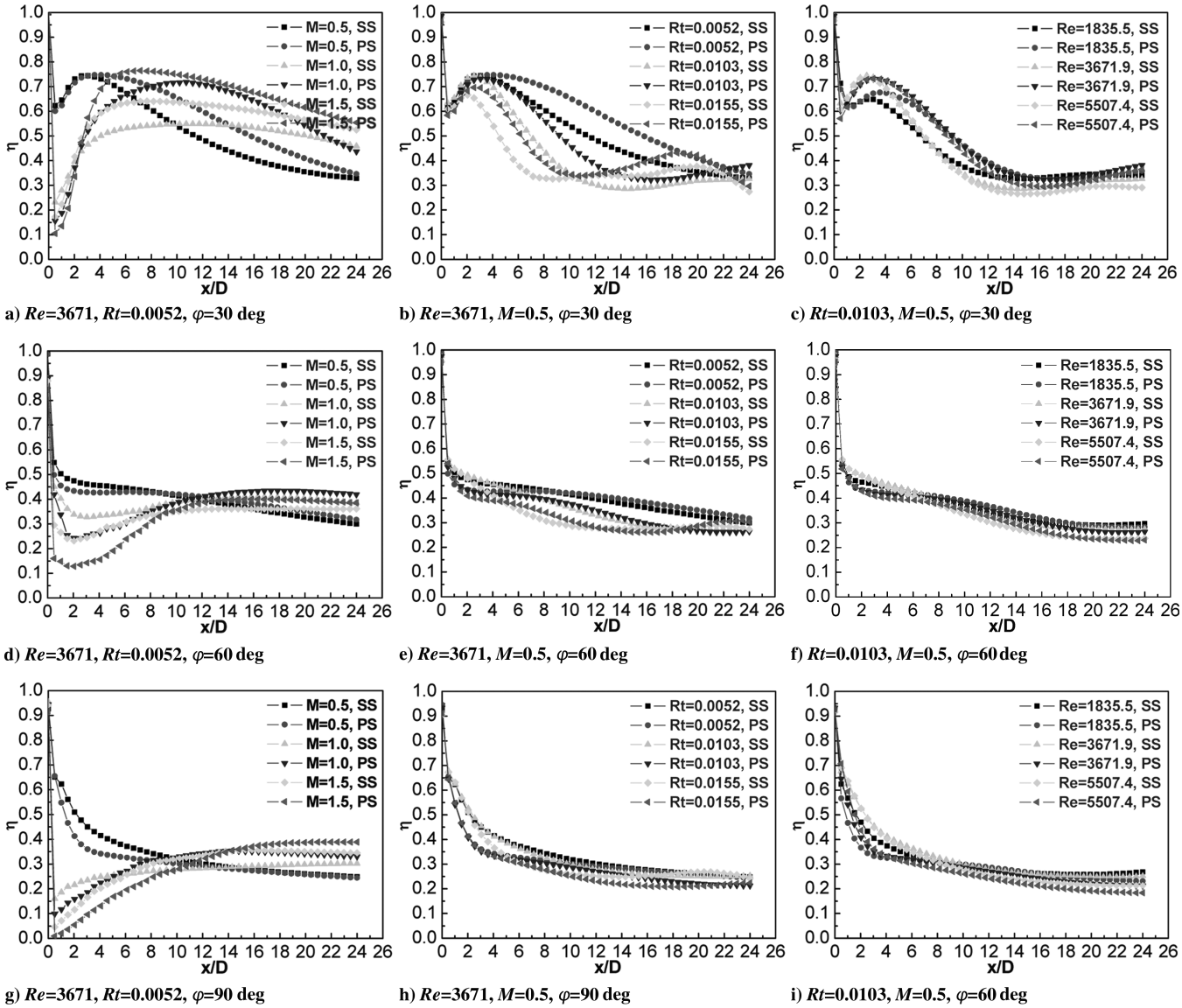

a) *Re*=3671, *Rt*=0.0052, φ=30 deg b) *Re*=3671, *M*=0.5, φ=30 deg c) *Rt*=0.0103, *M*=0.5, φ=30 deg

d) *Re*=3671, *Rt*=0.0052, φ=60 deg e) *Re*=3671, *M*=0.5, φ=60 deg f) *Rt*=0.0103, *M*=0.5, φ=60 deg

g) *Re*=3671, *Rt*=0.0052, φ=90 deg h) *Re*=3671, *M*=0.5, φ=90 deg i) *Rt*=0.0103, *M*=0.5, φ=60 deg

Fig. 8 Laterally averaged film-cooling effectiveness downstream of hole 6.

$$C_d = m \Big/ \left(P_{\text{tc}} \left(\frac{P_g}{P_{\text{tc}}} \right)^{\frac{k+1}{2k}} \left\{ \frac{2k}{(k-1)RT_{\text{tc}}} \left[\left(\frac{P_{\text{tc}}}{P_g} \right)^{\frac{k-1}{k}} - 1 \right] \right\}^{\frac{1}{2}} \frac{\pi}{4} D^2 \right) \tag{4}$$

where C_d depends on both the local geometry and flow conditions upstream and downstream of the cooling hole, such as the length-to-diameter ratio L/D, the pressure ratio across the hole, the angles of inclination φ, the exit geometry, etc. For the present study, the effects of M, Reynolds number, and Rt on C_d at three inclination angles are investigated. Figure 9 illustrates the distributions of C_d for all of the injection holes under different operating conditions. As can be seen in Fig. 9, the C_d values for each injection hole are quite different, and this denotes that the M is only a qualitative parameter for the distribution of total coolant mass flux in this study. All of the C_d groups decrease on both the suction surface and pressure surface as Rt is increased for a constant Reynolds number, and the C_d always increases with increasing M. This is due to the fact that when the M increases, the coolant can break away from the repression of the mainstream and flow out easily along the y direction. The rotation can always cause the pressure increase along the radial direction in the plenum, and this results in the accretion of P_{tc}, leading to an increscent difference between P_{tc} and P_g. Finally, C_d shows a decrease as Rt increases from 0.0103 to 0.0309. It can be seen that the Reynolds number shows no effect on C_d distributions at a fixed value of M and Rt (see Figs. 9c, 9f, and 9i), and this result also corresponds with the conclusion by Kim et al. [8]. The reason could be attributed to the synchronous variation of angular speed. In this figure, it is also demonstrated that C_d on the pressure surface is much higher than on the suction surface under each operating condition. The Coriolis force drives a majority of coolant to deviate from the suction surface in the plenum, causing more coolant discharge from the hole pipes on the pressure surface. Considering that there is no obvious difference in P_g near the two flat surfaces, as a consequence, the C_d values on the pressure surface are much higher. When comparing the results among three values of φ, the C_d values increase gradually on the pressure surface as the inclination angle φ varies from 30 to 90 deg, but this tendency is not apparent on the suction surface. In addition, C_d shows only a moderate variation along the radial direction, and the values in cooling holes 5–7 are slightly higher than others.

IV. Conclusions

Numerical simulations were performed to investigate the effect of rotation on the flow characteristics and film-cooling performance over a simplified rotating model. The computational model originates from the midspan section of a typical turbine rotor with two rows of 14 staggered injection holes on the suction surface and pressure surface, and Wilcox's κ-ω model is used for modeling the turbulence. The operating conditions include various values of

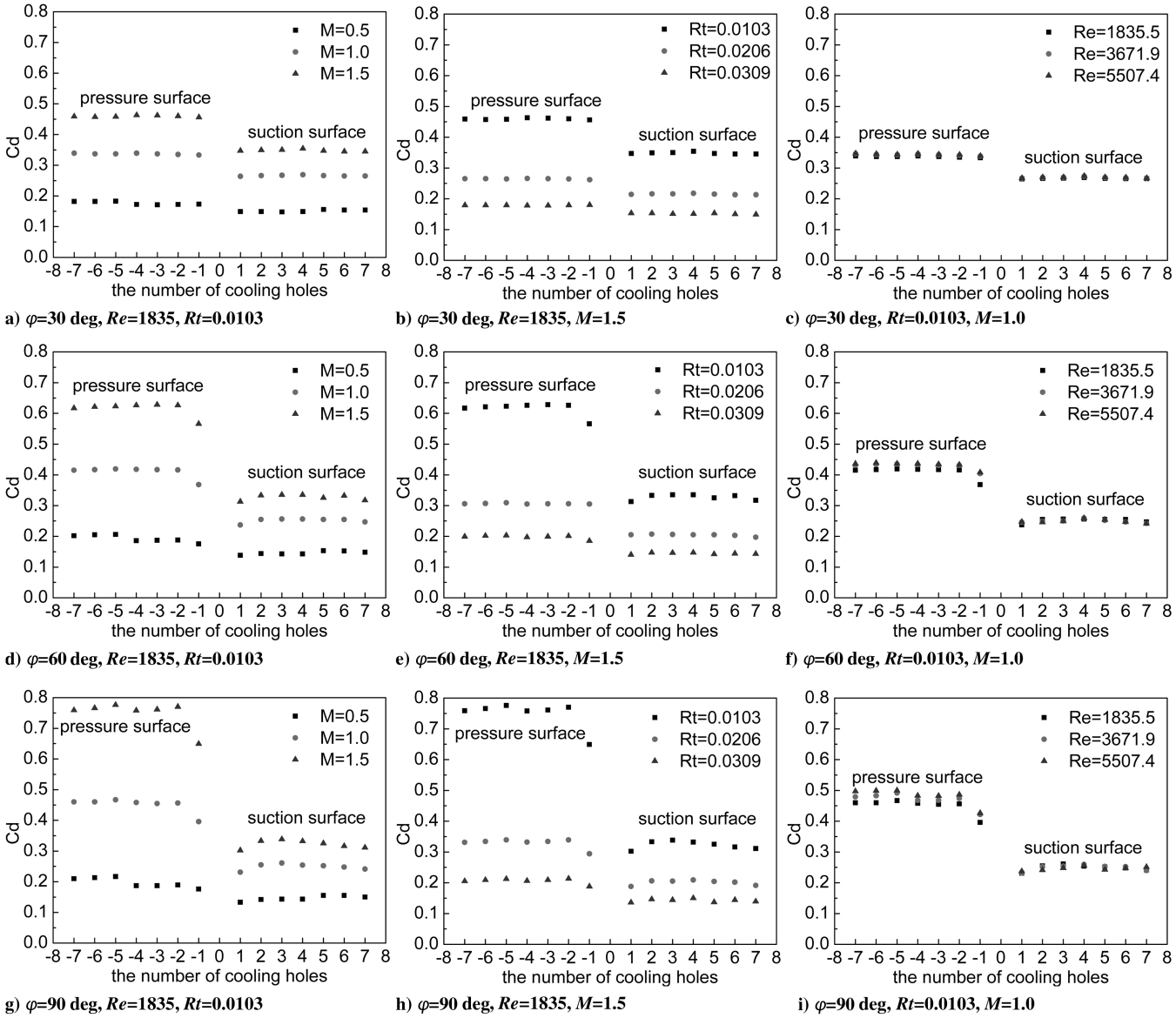

a) φ=30 deg, *Re*=1835, *Rt*=0.0103 b) φ=30 deg, *Re*=1835, *M*=1.5 c) φ=30 deg, *Rt*=0.0103, *M*=1.0

d) φ=60 deg, *Re*=1835, *Rt*=0.0103 e) φ=60 deg, *Re*=1835, *M*=1.5 f) φ=60 deg, *Rt*=0.0103, *M*=1.0

g) φ=90 deg, *Re*=1835, *Rt*=0.0103 h) φ=90 deg, *Re*=1835, *M*=1.5 i) φ=90 deg, *Rt*=0.0103, *M*=1.0

Fig. 9 Calculated C_d for all of the hole pipes.

Reynolds number *Re*, rotation number *Rt*, and averaged blowing ratio *M*, and the inclination angles to the suction and pressure surfaces are $\varphi = 30$, 60, and 90 deg, respectively. The key findings of the present study can be summarized as follows:

1) The rotational effect has a significant influence on the flowfield. The centrifugal force and Coriolis force have the same direction near the suction surface to point toward the high-radius locations, but the Coriolis force can weaken the centrifugal effect due to its opposite direction near the pressure surface. It is evident that the coolant is deflected upward along the radial direction in the present study. The critical values of angular speed (CAS) for equilibrium of the two governing forces near the pressure surface are also investigated.

2) Although the high values of *M* will weaken the thermal protection to wall surfaces near the exit of cooling holes, it can increase the adiabatic effectiveness properly at downstream locations. As the *Rt* increases, the values of η on both the suction surface and pressure surface decrease simultaneously. In addition, the augmentation of Reynolds number can lead to a slight decrease in η.

3) For discharge-coefficient distribution, in all cases, an increase in *Rt* leads to a decrease of C_d for a constant Reynolds number. The augmentation of *M* will always aid to elevate the C_d values. When *Rt* and *M* are fixed, the C_d values are independent of the variation of Reynolds number under a given operating condition. Furthermore, the C_d values on the pressure surface are much higher than those on the suction surface under the same operating condition.

4) Compared with the inclination angles of $\varphi = 60$ and 90 deg, the coolant at $\varphi = 30$ deg presents the best effective protection to wall surfaces.

Acknowledgments

The research herein was supported by the program of New Century Excellent Talents in Beihang University (grant no. NCET-05-0189) and was also partly funded by the Fanzhou Youth Science Foundation (grant no. 20070401).

References

[1] Goldstein, R. J., "Film-Cooling," *Advances in Heat Transfer*, Vol. 7, Academic Press, New York, 1971, pp. 321–379.

[2] Han, J. C., Dutta, S., and Ekkad, S. V., *Gas Turbine Heat Transfer and Cooling Technology*, Taylor and Francis, New York, 2000, pp. 129–243.

[3] Sinha, A. K., Bogard, D. G., and Crawford, M. E., "Gas Turbine Film-Cooling: Flowfield due to a Second Row of Holes," *Journal of Turbomachinery*, Vol. 113, No. 3, 1991, pp. 450–456. doi:10.1115/1.2927895

[4] Baldauf, S., Schulz, A., and Wittig, S., "High-Resolution Measurements of Local Effectiveness from Discrete Hole Film-Cooling," *Journal of Turbomachinery*, Vol. 123, No. 4, 2001, pp. 758–765. doi:10.1115/1.1371778

[5] Harrington, M. K., McWaters, M. A., Bogard, D. G., Lemmon, C. A.,

and Thole, K. A., "Full-Coverage Film-Cooling with Short Normal Injection Holes," *Journal of Turbomachinery*, Vol. 123, No. 4, 2001, pp. 798–805. doi:10.1115/1.1400111

[6] Ahn, J., Jung, I. S., and Lee, J. S., "Film-Cooling from Two Rows of Holes with Opposite Orientation Angles: Injectant Behaviors and Adiabatic Film-Cooling Effectiveness," *International Journal of Heat and Fluid Flow*, Vol. 24, No. 1, 2003, pp. 91–99. doi:10.1016/S0142-727X(02)00200-X

[7] Saumweber, C., and Schulz, A., "Interaction of Film Cooling Rows: Effects of Hole Geometry and Row Spacing on the Cooling Performance Downstream of the Second Row of Holes," *Journal of Turbomachinery*, Vol. 126, No. 2, 2004, pp. 237–246. doi:10.1115/1.1731395

[8] Kim, Y. W., Coon, C., and Moon, H. K., "Film-Cooling Characteristics of Pressure-Side Discharge Slots in an Accelerating Mainstream Flow," Proceedings of ASME Turbo Expo, American Society of Mechanical Engineers, Paper GT 2005-69061, 2005.

[9] Yuen, C. H. N., and Martinez-Botas, R. F., "Film-Cooling Characteristics of Rows of Round Holes at Various Streamwise Angles in a Crossflow. Part 1: Effectiveness," *International Journal of Heat and Mass Transfer*, Vol. 48, Nos. 23–24, 2005, pp. 4995–5016. doi:10.1016/j.ijheatmasstransfer.2005.05.019

[10] Yuen, C. H. N., and Martinez-Botas, R. F., "Film-Cooling Characteristics of Rows of Round Holes at Various Streamwise Angles in a Crossflow. Part 2: Heat Transfer Coefficients," *International Journal of Heat and Mass Transfer*, Vol. 48, Nos. 23–24, 2005, pp. 5017–5035. doi:10.1016/j.ijheatmasstransfer.2005.05.020

[11] Garg, V. K., and Gaugler, R. E., "Effect of Velocity and Temperature Distribution at the Hole Exit on Film-Cooling of Turbine Blades," *Journal of Turbomachinery*, Vol. 119, 1997, pp. 343–351.

[12] Garg, V. K., "Adiabatic Effectiveness and Heat Transfer Coefficient on a Film-Cooled Rotating Blade," *Numerical Heat Transfer, Part A, Applications*, Vol. 32, No. 8, 1997, pp. 811–830. doi:10.1080/10407789708913919

[13] Garg, V. K., and Gaugler, R. E., "Leading Edge Film-Cooling Effects on Turbine Blade Heat Transfer," *Numerical Heat Transfer, Part A, Applications*, Vol. 30, No. 2, 1996, pp. 165–187. doi:10.1080/10407789608913834

[14] Garg, V. K., and Gaugler, R. E., "Effect of Coolant Temperature and Mass Flow on Film-Cooling of Turbine Blades," *International Journal of Heat and Mass Transfer*, Vol. 40, No. 2, 1997, pp. 435–445. doi:10.1016/0017-9310(96)00040-3

[15] Leylek, J. H., and Zerkle, R. D., "Discrete-Jet Film-Cooling: A Comparison of Computational Results with Experiments," *Journal of Turbomachinery*, Vol. 116, No. 3, 1994, pp. 358–368. doi:10.1115/1.2929422

[16] Giebert, D., Gritsch, M., Schulz, A., and Wittig, S., "Film-Cooling from Holes with Expanded Exits: A Comparison of Computational Results with Experiments," ASME Turbo Expo, American Society of Mechanical Engineers, Paper 97-GT-163, 1997.

[17] Lakehal, D., Theodoridis, G. S., and Rodi, W., "Computation of Film Cooling of a Flat Plate by Lateral Injection from a Row of Holes," *International Journal of Heat and Fluid Flow*, Vol. 19, No. 5, 1998. pp. 418–430. doi:10.1016/S0142-727X(98)10022-X

[18] Azzi, A., and Lakehal, D., "Perspectives in Modeling Film-Cooling of Turbine Blades by Transcending Conventional Two-Equation Turbulence Models," *Journal of Turbomachinery*, Vol. 124, No. 3, 2002, pp. 472–484. doi:10.1115/1.1485294

[19] Garg, V. K., and Rigby, D. L., "Heat Transfer on a Film-Cooled Blade —Effect of Hole Physics," *International Journal of Heat and Fluid Flow*, Vol. 20, No. 1, 1999, pp. 10–25. doi:10.1016/S0142-727X(98)10048-6

[20] Tyagi, M., and Acharya, S., "Large Eddy Simulation of Film Cooling Flow from an Inclined Cylindrical Jet," *Journal of Turbomachinery*, Vol. 125, No. 4, 2003, pp. 734–742. doi:10.1115/1.1625397

[21] Muldoon, F., and Acharya, S., "Direct Numerical Simulation of a Film-Cooling Jet," ASME Turbo Expo, American Society of Mechanical Engineers, Paper GT2004-53502, 2004.

[22] Dring, R. P., Blair, M. F., and Joslyn, H. D., "An Experimental Investigation of Film Cooling on a Turbine Rotor Blade," *Journal of Engineering for Power*, Vol. 102, 1980, pp. 81–87; also American Society of Mechanical Engineers Paper ASME 79-GT-32.

[23] Takeishi, K., Aoki, S., Sato, T., and Tsukagoshi, K., "Film-Cooling on a Gas Turbine Rotor Blade," *Journal of Turbomachinery*, Vol. 114, No. 4, 1992, pp. 828–834. doi:10.1115/1.2928036

[24] Abhari, R. S., and Epstein, A. H., "An Experimental Study of Film Cooling in a Rotating Transonic Turbine," *Journal of Turbomachinery*, Vol. 116, 1994, pp. 63–70. doi:10.1115/1.2928279

[25] Ahn, J., Schobeiri, M. T., Han, J. C., and Moon, H. K., "Film-Cooling Effectiveness on the Leading Edge of a Rotating Film-Cooled Blade Using Pressure-Sensitive Paint," ASME Turbo Expo, American Society of Mechanical Engineers, Paper GT 2005-68344, 2005.

[26] Ahn, J., Schobeiri, M. T., Han, J. C., and Moon, H. K., "Effect of Rotation on Leading Edge Region Film-Cooling of a Gas Turbine Blade with Three Rows of Film Cooling Holes," *International Journal of Heat and Mass Transfer*, Vol. 50, Nos. 1–2, 2007, pp. 15–25. doi:10.1016/j.ijheatmasstransfer.2006.06.028

[27] Yang, H. T., Chen, H. C., Han, J. C., and Moon, H. K., "Numerical Prediction of Film Cooling and Heat Transfer on the Leading Edge of a Rotating Blade with Two Rows Holes in a 1-$\frac{1}{2}$ Turbine Stage at Design and Off Design Conditions," ASME Turbo Expo, American Society of Mechanical Engineers, Paper GT2005-68335, 2005.

[28] Garg, V. K., and Abhari, R. S., "Comparison of Predicted and Experimental Nusselt Number for a Film-Cooled Rotating Blade," *International Journal of Heat and Fluid Flow*, Vol. 18, No. 5, 1997, pp. 452–460. doi:10.1016/S0142-727X(97)00031-3

[29] Garg, V. K., "Heat Transfer on a Film-Cooled Rotating Blade Using Different Turbulence Models," *International Journal of Heat and Mass Transfer*, Vol. 42, No. 5, 1999, pp. 789–802. doi:10.1016/S0017-9310(98)00229-4

[30] Garg, V. K., "Heat Transfer on a Film-Cooled Rotating Blade," *International Journal of Heat and Fluid Flow*, Vol. 21, No. 2, 2000, pp. 134–145. doi:10.1016/S0142-727X(99)00072-7

[31] Garg, V. K., "Modeling Film-Coolant Flow Characters at the Exit of Shower-Head Holes," *International Journal of Heat and Fluid Flow*, Vol. 22, No. 2, 2001, pp. 134–142. doi:10.1016/S0142-727X(00)00083-7

[32] Garg, V. K., and Ameri, A. A., "Two-Equation Turbulence Models for Prediction of Heat Transfer on a Transonic Turbine Blade," *International Journal of Heat and Fluid Flow*, Vol. 22, No. 6, 2001, pp. 593–602. doi:10.1016/S0142-727X(01)00128-X

[33] Hoda, A., and Acharya, S., "Predictions of a Film-Cooling Jet in Crossflow with Different Turbulent Models," *Journal of Turbomachinery*, Vol. 122, No. 3, 2000, pp. 558–569. doi:10.1115/1.1302322

[34] Wilcox, D. C., *Turbulence Modeling for CFD*, 2nd ed., DCW Industries, Inc., La Canada, CA, 1998.

[35] Bohn, D., Ren, J., and Kusterer, K., "Conjuate Heat Transfer Analysis for Film-Cooling Configurations for Different Hole Geometries," ASME Turbo Expo, American Society of Mechanical Engineers, Paper GT 2003-38369, 2003.